*Progress In Electromagnetics Research C, Vol. 85, 191–208, 2018*

# A Compact Conformal Printed Dipole Antenna for 5G Based Vehicular Communication Applications

**Yalavarthi Usha Devi[1, 2, *], Mulpuri S. S. Rukmini[1], and Boddapati T. P. Madhav[2]**

**Abstract**—A novel and compact conformal printed dipole antenna with geometrical modifications in ground plane is proposed in this paper for 5G based vehicular communications and IoT applications. The proposed antenna consists of a printed dipole as defected ground structure and a staircase structured offset fed integrated balun to attain wideband operation. It yields a better −10 dB impedance bandwidth of 17.65 GHz and 2.24 GHz over the frequency ranges 24.3 to 41.95 GHz and 49.91 to 2.15 GHz. Antenna projects the peak gain of 6.81 dB with 98.82% of peak radiation efficiency. The measured results of the proposed model are in good agreement with the simulation obtained from HFSS. The conformal models of the proposed antenna are developed to embed the antenna in different curved surfaces on vehicular body. The analyzed conformal characteristics of the antenna support excellent constant reflection coefficient with respect to planar structure of the antenna over the operating band at different angles.

## 1. INTRODUCTION

Vehicular communications play a vital role in intelligent transportation system (ITS). It will lead to no collision, low traffic congestion, reduced fuel and energy consumption transportation system. IoV-Internet of Vehicles emerges from the concept of integrating IoT (Internet of Things) with connected vehicles. In IoV, the vehicular communications may be from vehicle to vehicle, vehicle to infrastructure, vehicle to roadside unit, vehicle to pedestrian or vehicle to network. The use of 5G and mm-waves in vehicular communications will improve the data rates, capacity and reliability for vehicular networks [1]. Fig. 1 describes the improvement in performance, capacity and change in frequency bands for wireless and mobile communication applications.

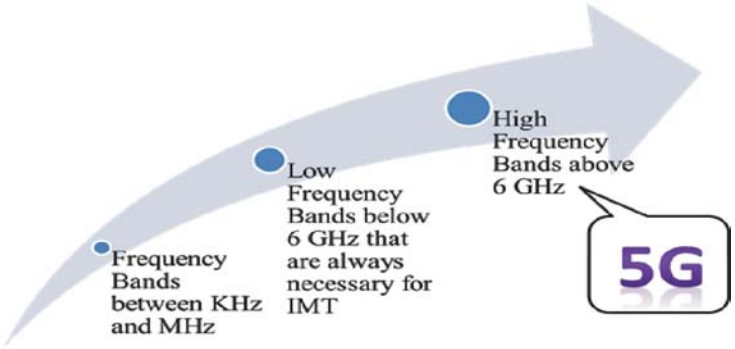


**Figure 1.** Advancements in frequency bands for wireless and mobile communications.

*Received 19 April 2018, Accepted 10 July 2018, Scheduled 23 July 2018*
* Corresponding author: Yalavarthi Usha Devi (ushadevi.yalavarthi@kluniversity.in).
[1] Department of ECE, VFSTR, AP, India. [2] Department of ECE, Koneru Lakshmaiah Education Foundation, AP, India.

After the most recent World Radio-Communications Conference (WRC), the ITU released the following list of proposed globally viable frequencies between 24 GHz and 86 GHz for future development of IMT application (International Mobile Telecommunications): 24.25–27.5 GHz, 31.8–33.4 GHz, 37–40.5 GHz, 40.5–42.5 GHz, 45.5–50.2 GHz, 50.4–52.6 GHz, 66–76 GHz and 81–86 GHz [2]. Fig. 2 represents the scenario of vehicular communications in ITS. The existing 4G cellular systems and the DSRC (Dedicated Short-Range Communications) spectrum allocated for vehicular communications have certain limitations for future connected vehicles [3]. The significance of mm waves and 5G frequency bands for communications in vehicular technology are described by the authors in [3] and [4]. To facilitate this, FCC has proposed to authorize the operation in 28, 37 and 39 GHz of licensed band, and 64–71 GHz band is made available for unlicensed spectra for mobile use [3]. 5G wireless will assure smart and intelligent vehicular communications with low latency, high bandwidth and pervasive availability.

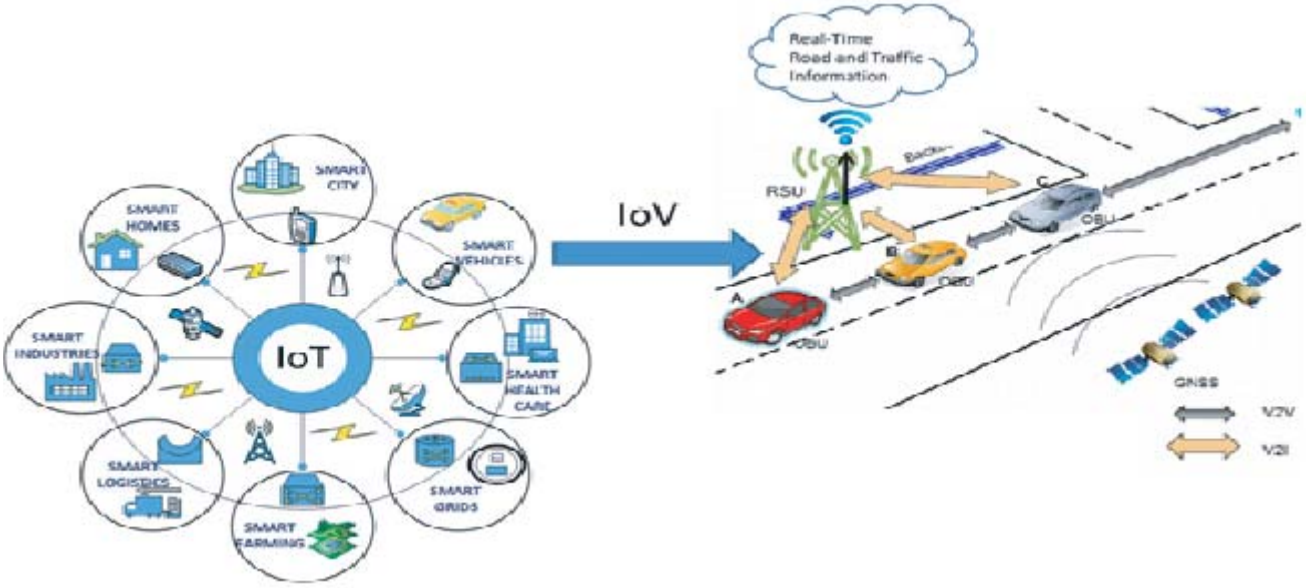


**Figure 2.** Applications of IoT and scenario of intelligent transportation.

Various antennas were proposed in previous works that achieved 5G frequencies mostly 28 GHz and 33 GHz [5–11]. A low profile insensitive air-filled slot-loop antenna for 5G is designed [5], and it operates from 21 to 23.5 GHz. A rectangular Dielectric Resonator Antenna (RDRA) at 28 GHz is designed [6]. It offers a bandwidth of 2.1 GHz from 27.0 to 29.1 GHz and gain of 12.1 dB. An omnidirectional circularly polarized antenna at 28 GHz is designed for D2D communications [7]. It operates from 26.5 to 28.7 GHz with 8% fractional bandwidth. A microstrip fed end-fire angled dipole antenna is developed [8]. It provides a wide bandwidth from 20 to 26 GHz with a gain about 2.5 dB. The gain is further enhanced by using a corrugated ground plane. A printed dipole antenna angled at 45° with broad band characteristics is proposed [9]. It operates for a wide band of 26.5–38.2 GHz with a gain of 4.9–5.9 dBi. It is further enhanced by extending the proposed antenna as a beam-forming radiator with a 8-element linear array [10]. Wider scanning angle and higher gain are achieved due to the presence of stubs in array. A triple band mm-wave 2D array antenna based on enhanced Franklin Antenna is designed [11]. It operates at 28 GHz, 33 GHz as well as from 37 to 39 GHz with considerable gains.

Different antenna designs for various communication technologies such as LTE (Long Term Evolution), DSRC, WLAN, WiMAX, GPS were proposed in [12–17]. A compact integrated Bluetooth antenna with notch band characteristics for automotive applications is presented in [12]. A transparent conformal wheel-shaped fractal antenna is proposed in [13] for vehicular communication applications. A spiral antenna with circular polarization is proposed to work at frequencies 1.2, 1.5, 2.4, 3.3 and 5.8 GHz for vehicular mobile communications [14]. Mondal et al. proposed a tri-band hexagonal microstrip

antenna [15] to be integrated in smart vehicles for short range communication. This antenna works for GPS, WiMAX and DSRC bands. A monopolar patch antenna with V-shaped slot is proposed in [16] for car to car and WLAN communications.

This paper proposes a printed dipole antenna with an offset fed staircase structure integrated with balun and printed dipole as DGS. It operates from 24.3 to 41.95 GHz and 49.91 to 52.15 GHz. The 5G frequencies 28, 33, 37 and 39 GHz can be used for future vehicular communications as proposed by FCC [3], and 51 GHz can be used for future satellite applications [2]. The proposed antenna iterations and geometry are described in Section 2. Section 3 gives the design considerations of the proposed antenna. Section 4 presents the simulated and measured results of the proposed antenna in terms of $S_{11}$ parameters, current distribution, radiation patterns, gain, efficiency, and comparison with previous relevant works. Section 5 describes the developed conformal models and placement of the proposed antenna on the vehicle with respective results.

## 2. ANTENNA DESIGN

For better impedance matching and to achieve broad frequency range, an integrated balun is used as a center feed structure in the antenna design. The ground plane is truncated, and a printed dipole is angled at 45° on the truncated ground plane. A rectangular slot is etched on ground plane in between the folded microstrip line of balun structure. To further enhance the operating bandwidth, the center feed is modified to offset feed. The final proposed antenna model consists of a truncated ground plane, an integrated balun as offset feed with staircase structure and a printed dipole angled at 45°. The antenna iterations are shown in Fig. 3, and the geometry of final proposed antenna model is given in Fig. 4(a). The design parameters of proposed antenna are given in Table 1.

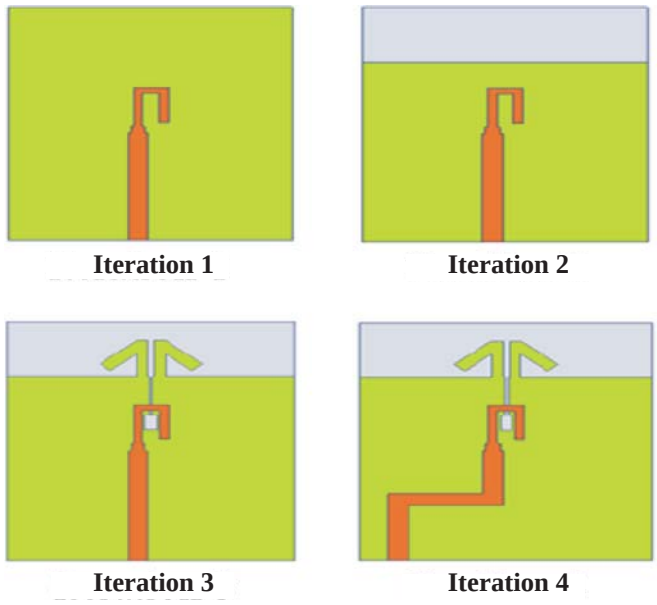


**Figure 3.** Designed antenna iterations.

The proposed antenna is built on both sides of Liquid crystal polymer sheet with dimension of $10 \times 13 \times 0.254\,\text{mm}^3$. Liquid crystal polymer consists of dielectric constant 2.9 with loss tangent of 0.002. LCP has low water vapor transition, low coefficient of thermal expansion and is non-flammable and flexible. The fabricated antenna is shown in Fig. 4(b). All the antenna iterations are simulated in EM (Electro-Magnetic) solver ANSYS HFSS.

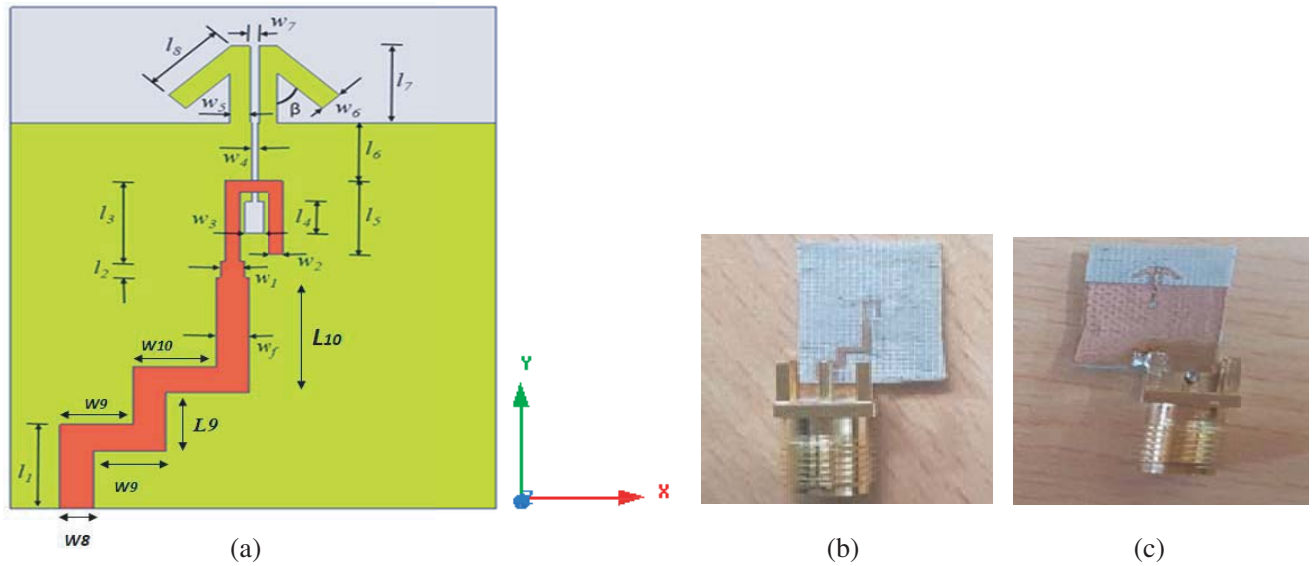


(a) (b) (c)

**Figure 4.** Fabricated antenna. (a) Proposed antenna, Iteration 5. (b) Top view. (c) Bottom view.

**Table 1.** Design parameters of proposed antenna model.

| Parameter | Size (mm) | Parameter | Size (mm) | Parameter | Size (mm) |
|---|---|---|---|---|---|
| $L_s$ | 13 | $W_s$ | 10 | $h$ | 0.254 |
| $l_1$ | 1.5 | $l_2$ | 0.4 | $l_3$ | 2.1 |
| $l_4$ | 0.8 | $l_5$ | 1.9 | $l_6$ | 1.2 |
| $l_7$ | 2 | $l_8$ | 1.8 | $l_9$ | 1.5 |
| $w_f$ | 0.68 | $w_1$ | 0.5 | $w_2$ | 0.3 |
| $w_3$ | 0.4 | $w_4$ | 0.1 | $w_5$ | 0.4 |
| $w_6$ | 0.5 | $w_7$ | 0.2 | $w_8$ | 0.7 |
| $w_9$ | 1.5 | $w_{10}$ | 1.7 | $l_{10}$ | 3 |

## 3. DESIGN CONSIDERATIONS

The important design parameters of microstrip and printed dipole antennas are operating wavelength, guide wavelength, relative dielectric constant, effective dielectric constant, thickness of the substrate, width of strip, effective length, length of dipole and width of dipole. The operating wavelength $\lambda_0$ is calculated as given in Equation (1), where

'$f_r'$ is the resonant frequency,

'$c$' is the velocity of light in free space.

$$\lambda_0 = c/f_r \tag{1}$$

Guide wavelength is given by:

$$\lambda_d = \lambda_0/\sqrt{\varepsilon_r} \tag{2}$$

where $\varepsilon_r$ is the relative dielectric constant.

The thickness of the substrate is given by:

$$h \leq \frac{0.3 * c}{2\pi f_r \sqrt{\varepsilon_r + 1}} \tag{3}$$

The width of the basic microstrip feed line is given by:

$$w = \frac{c}{2f_r}\sqrt{\frac{2}{\varepsilon_r + 1}} \tag{4}$$

The effective dielectric constant is calculated as:

$$\varepsilon_{reffective} = \frac{\varepsilon_r + 1}{2} + \frac{\varepsilon_r - 1}{2}\left[\left(1 + \frac{12h}{w}\right)^{-\frac{1}{2}} + 0.04\left(1 - \frac{w}{h}\right)^2\right] \tag{5}$$

The effective length due to effective dielectric constant is:

$$\Delta L = 0.412 * h\left\{\frac{\varepsilon_r + 0.3}{\varepsilon_r - 0.258}\right\}\left\{\frac{w/h + 0.264}{w/h + 0.813}\right\} \tag{6}$$

The length of the dipole is:

$$2l_8 = \left\{\frac{c}{2f_r\sqrt{\varepsilon_{reff}}}\right\} - 2\Delta L \tag{7}$$

The width of the dipole is:

$$w_6 = l_8/3 \tag{8}$$

Equations (1) to (8) are the design equations considered for the proposed antenna model [17, 18]. These parameters are adjusted during simulation, to get the optimum results.

## 4. RESULTS AND ANALYSIS

Figure 5 shows the reflection coefficient characteristics of above iterations and proposed antenna model in dB as a function of frequency in GHz. The simulated −10 dB impedance bandwidth of the proposed antenna model is 17.65 GHz from 24.3 to 41.95 GHz and 2.24 GHz from 49.91 to 52.15 GHz. It covers the 5G frequency bands 28 GHz, 33 GHz, 37 GHz and 39 GHz proposed by FCC for future vehicular communications. It also works at 51 GHz band, which is suitable for future satellite applications as released by ITU in the recent WRC [2].

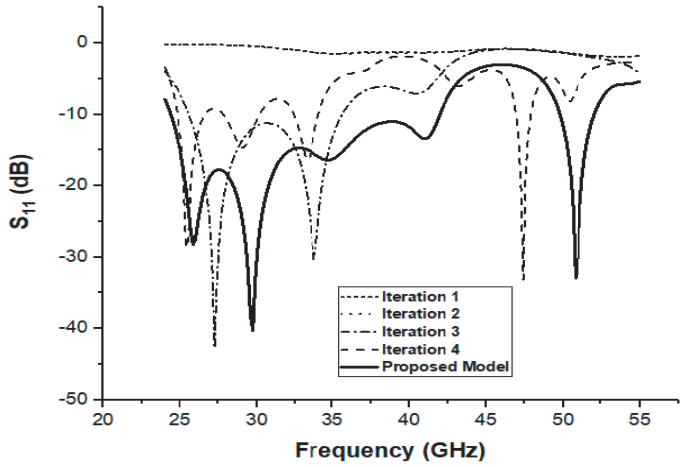


**Figure 5.** Simulated reflection coefficient curves for different iterations and proposed model.

### 4.1. Parametric Analysis

To obtain the optimum results, parametric analysis is done for feed width $W_f$ and width of dipole $W_5$. The simulated impedance bandwidth characteristics for variations in feed width are presented in Fig. 6. The values taken for analysis are 0.66 mm, 0.68 mm, 0.70 mm and 0.72 mm. For $W_f = 0.68$ mm, more operating bands are achieved. Fig. 7 illustrates the simulated reflection coefficient curves for variations in the width of dipole. The dipole width is varied from 0.3 mm to 0.6 mm with a step size of 0.1 mm. As illustrated in Fig. 7, $W_5 = 0.4$ mm achieves better operating band. Thus, for $W_f = 0.68$ mm and $W_5 = 0.4$ mm optimum results are obtained. The measured $S_{11}$ characteristics against the simulated one are presented in Fig. 8. Though the measured values deviate a little from that of simulated, the proposed antenna still achieves the required 5G bands.

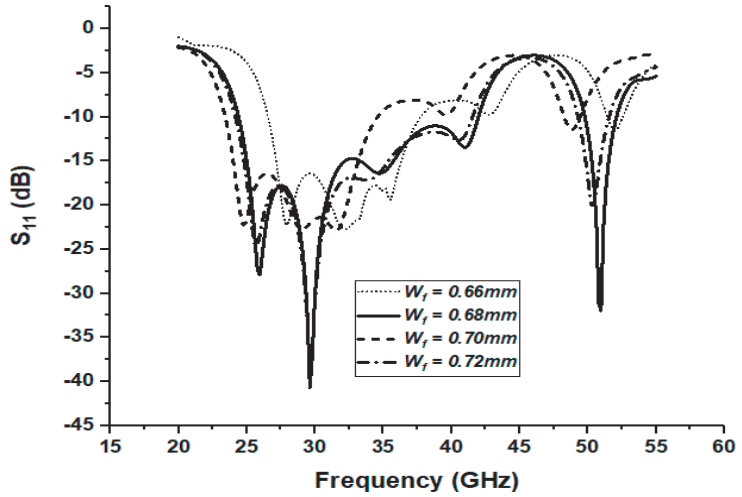


**Figure 6.** Simulated reflection coefficient curves for variations in $W_f$.

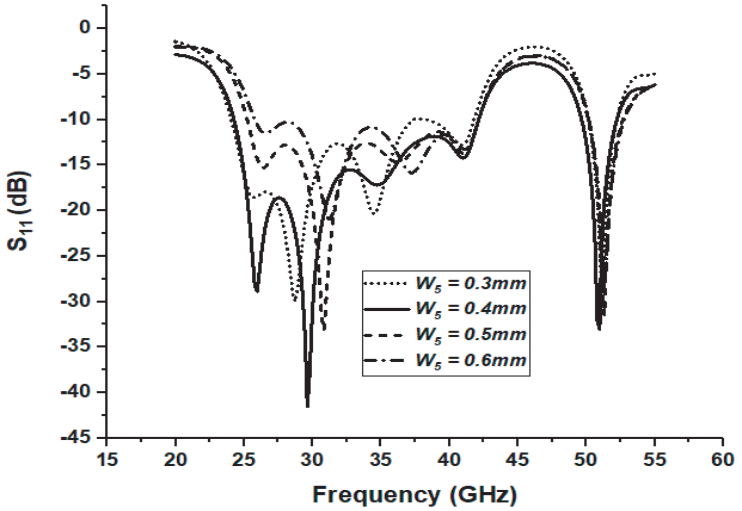


**Figure 7.** Simulated reflection coefficient curves for variations in $W_5$.

### 4.2. Current Distribution

The surface current distributions of the proposed antenna are shown in Fig. 9 at frequencies 28 GHz, 33 GHz, 37 GHz, 39 GHz and 51 GHz respectively. It can be observed that the current distributions on the microstrip feedline integrated with balun are not uniform and cancel each other in opposite directions. It does not radiate and acts as microstrip to slot line transformer where the etched rectangular slot on the ground plane couples to the folded microstrip line connected to the feedline. The current distributions on both sides of feed in the ground plane are in the same directions. The left side currents radiate through the left arm of angled dipole, and the right-side currents radiate through the right arm of the angled dipole along with the currents from etched rectangular slot. At 28 GHz, the maximum current distribution is observed at vertical staircase of balun structure. At 33 GHz, the current distribution is as that at 28 GHz, and maximum current is also observed near the dipoles. The current distributions at 37 GHz and 39 GHz are almost similar. The maxima are observed at horizontal staircase of balun structure and near dipoles at 39 GHz. The proposed antenna shows maximum current distribution almost throughout the balun structure at 51 GHz.

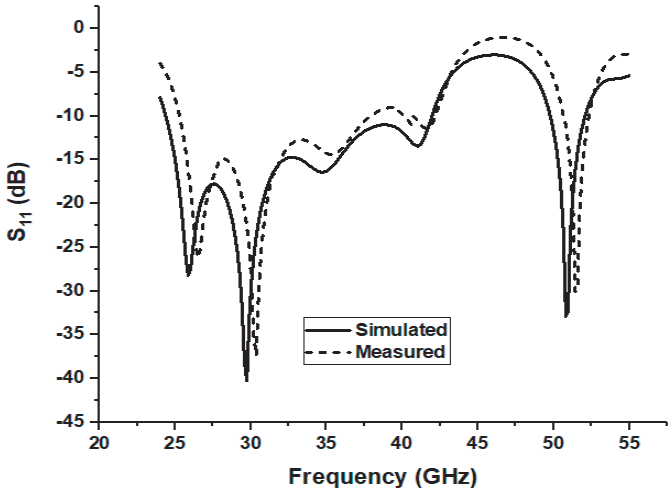


**Figure 8.** Measured and simulated reflection coefficient curves of proposed antenna.

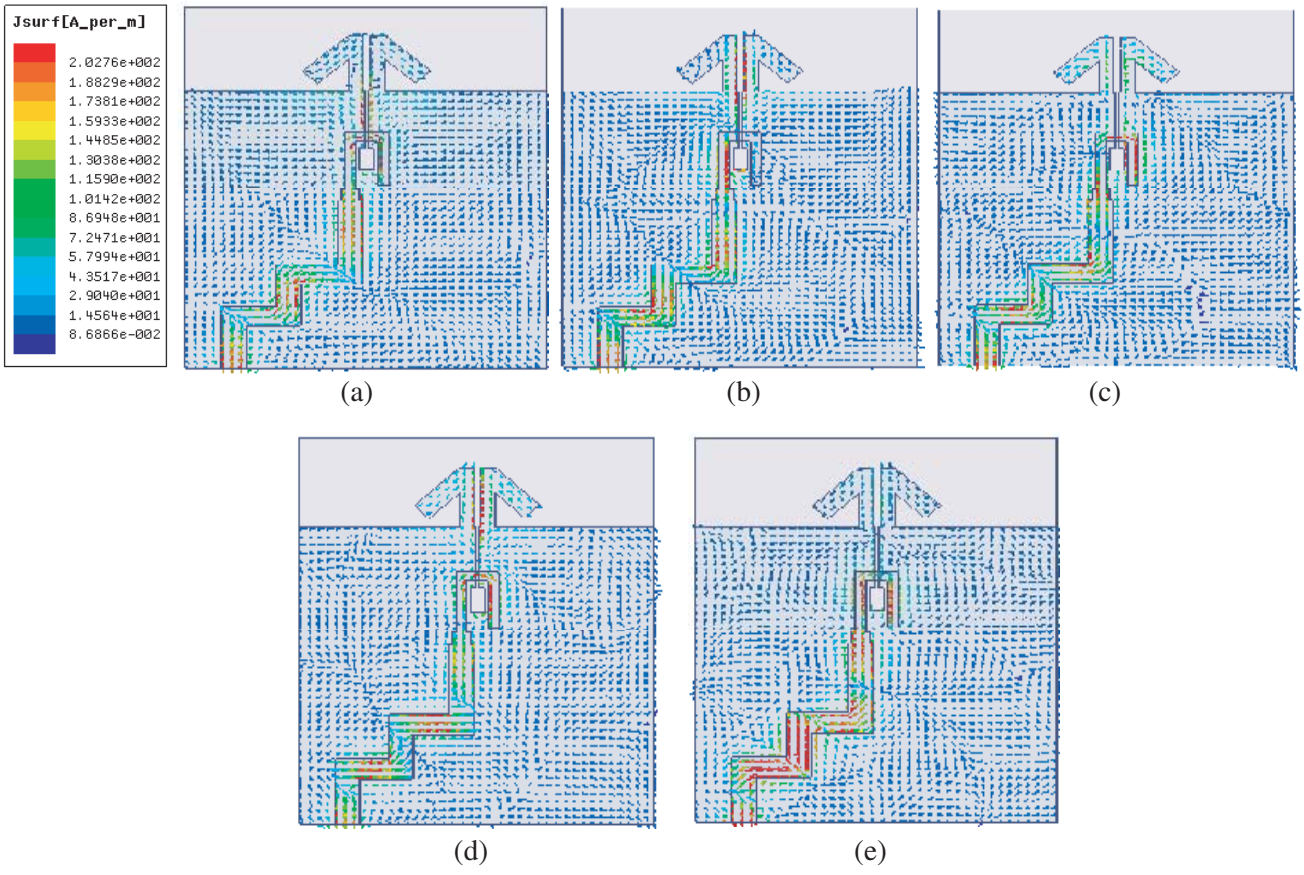


**Figure 9.** Current distribution for different resonant frequencies. (a) 28 GHz. (b) 33 GHz. (c) 37 GHz. (d) 39 GHz. (e) 51 GHz.

### 4.3. Radiation Pattern

The 3D gain plots at 28 GHz, 33 GHz, 37 GHz, 39 GHz and 51 GHz are illustrated in Fig. 10. The gains achieved are considerably good. From the plots obtained, the gain in dB at 28 GHz is 3.53 dB, 4.24 dB at 33 GHz, 3.71 dB at 37 GHz, 2.49 dB at 39 GHz and 6.59 dB at 51 GHz.

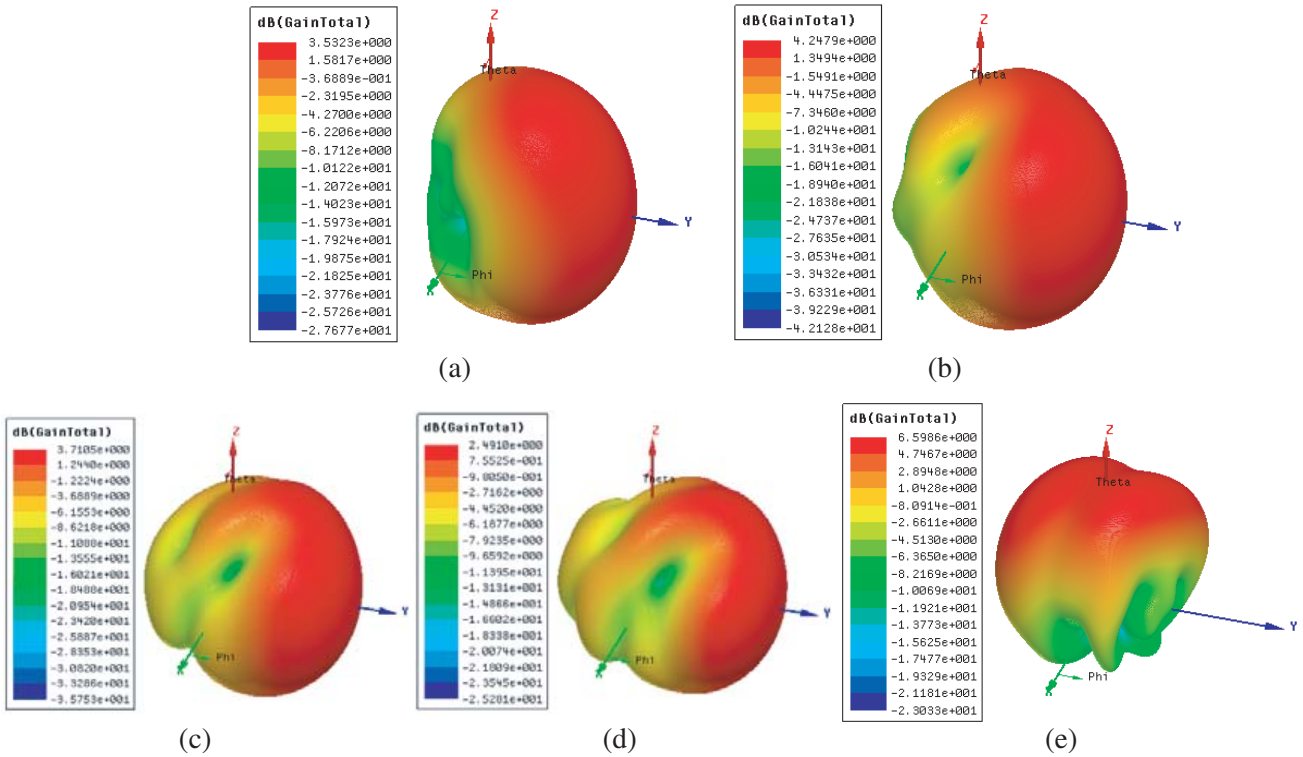


**Figure 10.** 3D Gain plots of proposed antenna. (a) 3D Gain at 28 GHz. (b) 3D Gain at 33 GHz. (c) 3D Gain at 37 GHz. (d) 3D Gain at 39 GHz. (e) 3D Gain at 51 GHz.

The simulated and measured radiation patterns are illustrated in Fig. 11 both for (i) $E$-plane and (ii) $H$-plane for resonant frequencies 28, 33, 37, 39 and 51 GHz. At 28 GHz the $E$-plane pattern is like dipole pattern while the patterns are directional at 33, 37, 39 and 51 GHz. The $H$-plane pattern is omnidirectional at 28 and 51 GHz. It is quasi-omni directional at 33 and 37 GHz and non-omnidirectional at 39 GHz.

### 4.4. Gain and Radiation Efficiency

The plot for frequency vs gain is shown in Fig. 12. From the plot, the maximum gain achieved is 6.81 dB at 51.15 GHz. Fig. 13 represents the frequency vs radiation efficiency plot obtained in simulation. It ranges from 97 to 98.82% over the frequency range of 24 to 55 GHz. The maximum radiation efficiency obtained is 98.82% at 28 GHz.

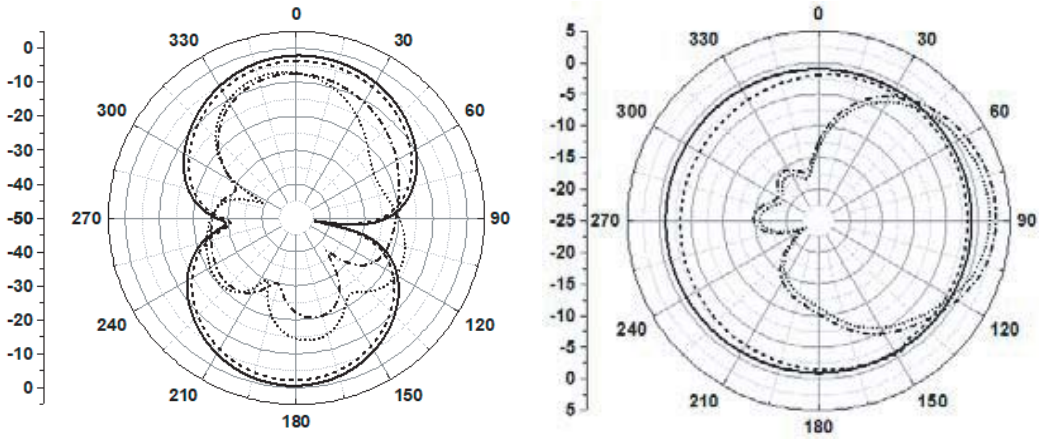

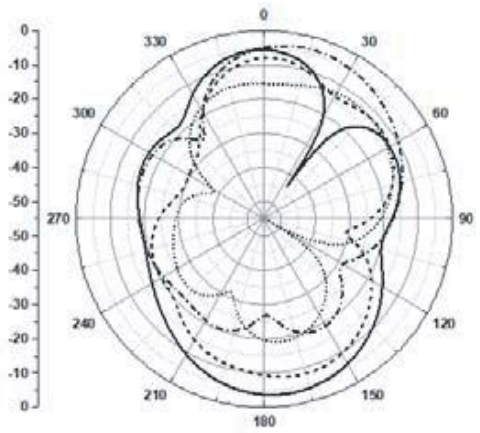


(i)

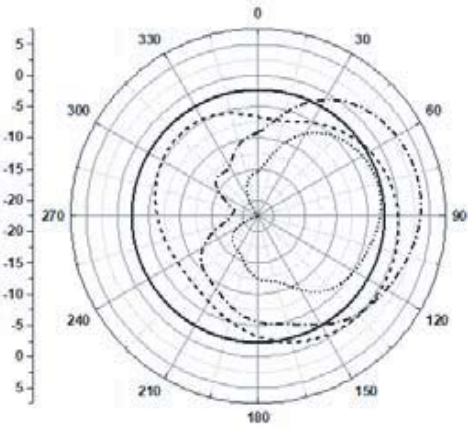


(ii)

(b)

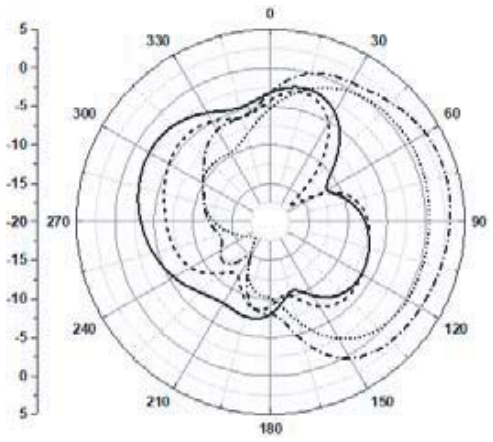


(i)

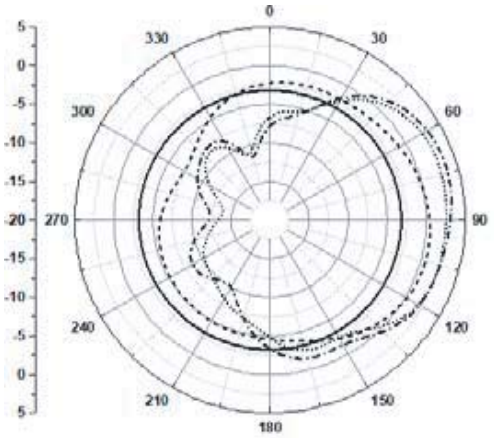


(ii)

(c)

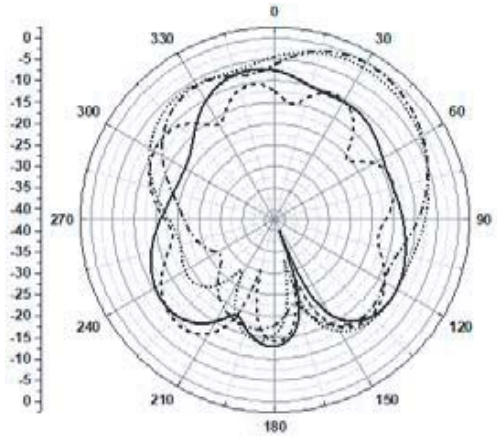


(i)

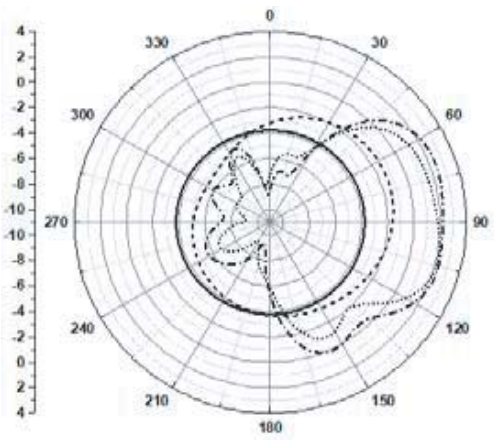


(ii)

(d)

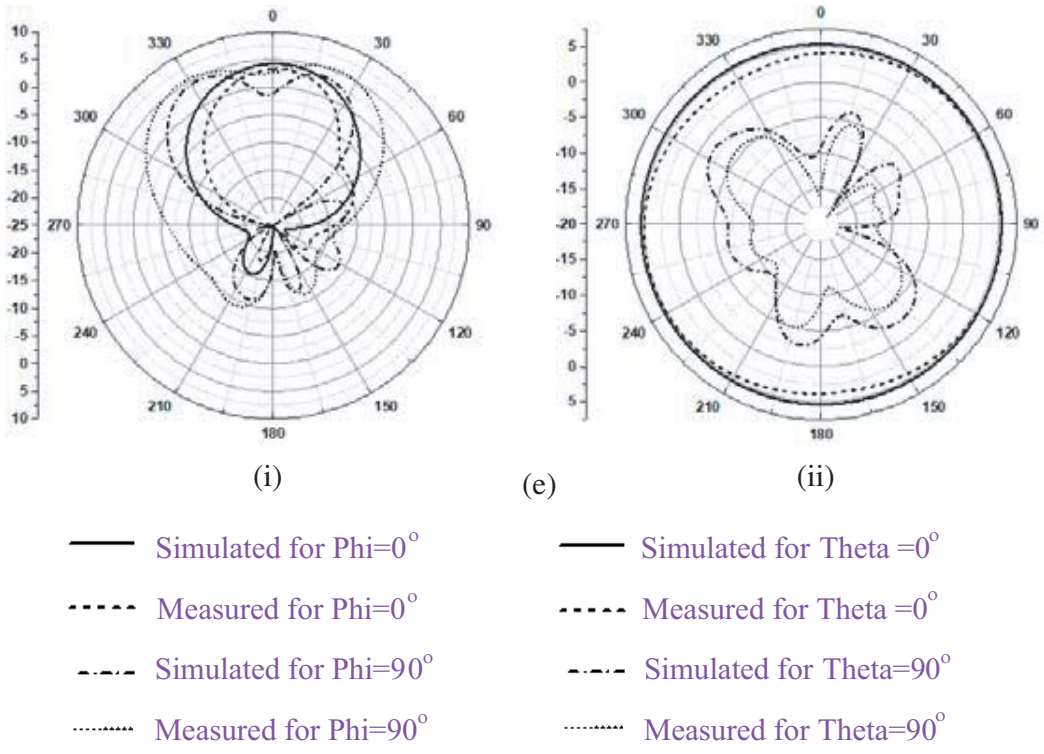


**Figure 11.** Radiation patterns in (i) *E*-Plane and (ii) *H*-Plane for different resonant frequencies. (a) 28 GHz. (b) 33 GHz. (c) 37 GHz. (d) 39 GHz. (e) 51 GHz.

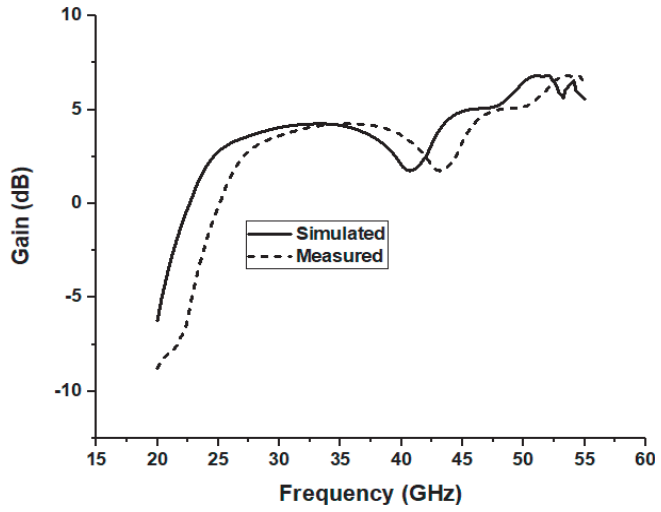


**Figure 12.** Gain vs frequency.

### 4.5. Antenna Parameters Comparison

The parameters: antenna dimensions, operating frequency bands, bandwidth, peak gain and efficiency of the proposed antenna are tabulated in Table 2 in comparison with the previous works published by various authors. From Table 2 it can be observed that the miniature sized proposed antenna has better −10 dB impedance bandwidth, peak gain and efficiency. The proposed antenna covers 5G bands of 28 GHz, 33 GHz, 37 GHz and 39 GHz for vehicular communications as proposed by FCC.

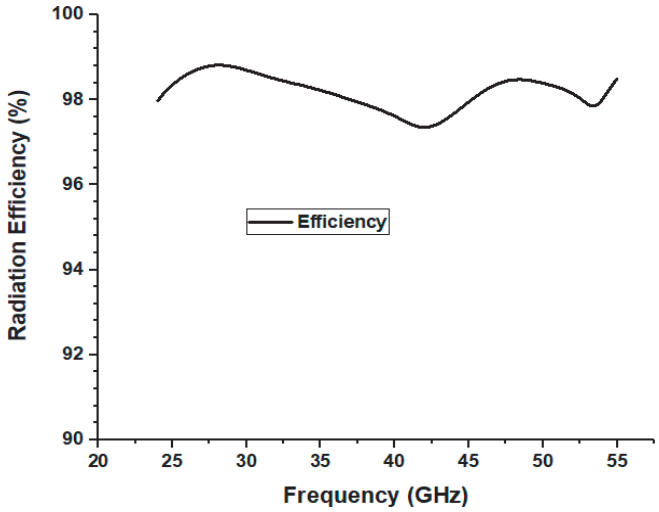


**Figure 13.** Radiation efficiency vs frequency.

**Table 2.** Comparison of planar antenna parameters with literature.

| R. No. | Antenna Dimensions (mm) $w \times l \times h$ | Operating Bands (GHz) | Bandwidth (GHz) | Peak Gain (dB) | Efficiency |
|---|---|---|---|---|---|
| [5] | $5 \times 10 \times 0.8$ | 21–23.5 | 2.5 | 5.9 | 95 |
| [6] | $11 \times 12 \times 0.254$ | 27–29.1 | 2.1 | 6.17 | 92 |
| [8] | $h = 0.381$ | 20–26 | 6 | 2.6 | 93 |
| [10] | $h = 0.254$ | 26.5–38.2 | 11.7 | 6.12 | 93 |
| Proposed Model | $10 \times 13 \times 0.254$ | 24.3–41.95, 49.91–52.15 | 17.65, 2.24 | 6.81 | 98.82 |

## 5. CONFORMAL STRUCTURES

An antenna that conforms to a curved surface or host body is known as conformal antenna. The designed antenna has low weight, easy fabrication and looking like the most suitable for embedding or installing in a wide variety of curved surfaces. It is very compact in dimension of $10 \times 13\,\text{mm}^2$ with thickness of 0.254 mm and can be integrated on vehicle structures. Hopefully it eliminates the antenna projection from surface of vehicles and reduces the aerodynamic drag and the error caused by radomes in vehicles. The conformal models of the proposed antenna are developed in simulation for different bending angles at 30°, 45°, 60°, and 90°. Fig. 14 illustrates the conformal models in HFSS. As the central angle increases, the radius of curvature decreases, and hence the antenna structure bends more.

Figure 15 presents the measured reflection coefficient vs frequency characteristics for basic un-bended model and conformal models at 30° and 45°. It is observed that both the conformal models also have similar impedance bandwidth to that of basic un-bended model with minor shift in frequencies. The basic flat model operates from 24.3 to 41.95 GHz and 49.91 to 52.15 GHz with bandwidths of 17.65 GHz and 2.24 GHz, respectively. The conformal model at 30° operates from 25.62 to 42.51 GHz and 49.53 to 52.05 GHz with respective bandwidths of 16.33 GHz and 2.52 GHz. The conformal model at 45° operates from 25.59 to 42.51 GHz with a bandwidth of 16.92 GHz and 50.55 to 53 GHz with a bandwidth of 2.45 GHz.

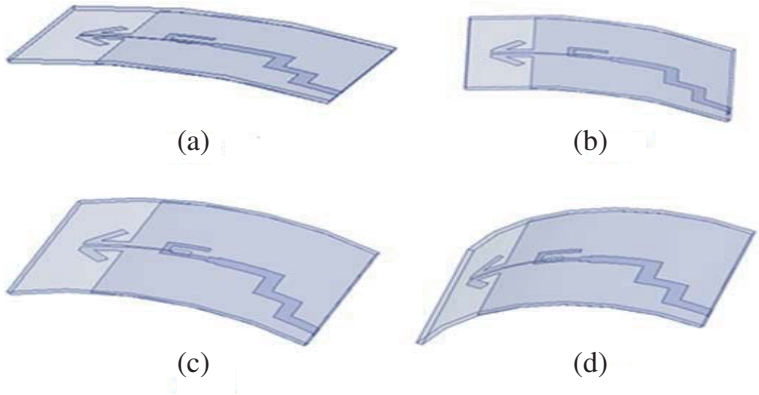


**Figure 14.** Conformal models in HFSS. (a) 30°. (b) 45°. (c) 60°. (d) 90°.

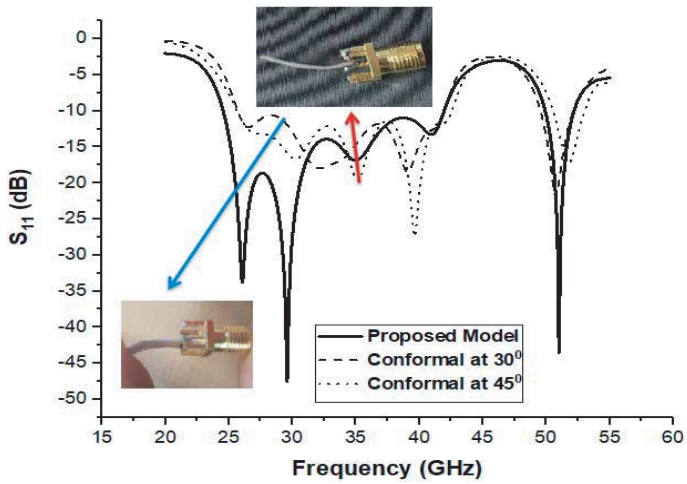


**Figure 15.** Reflection coefficient curves of Un-bended and conformal models at 30° and 45°.

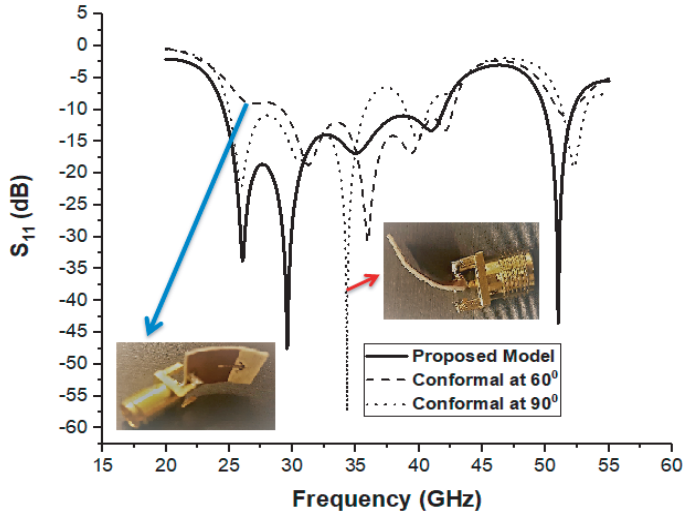


**Figure 16.** Reflection coefficient curves of Un-bended and conformal models at 60° and 90°.

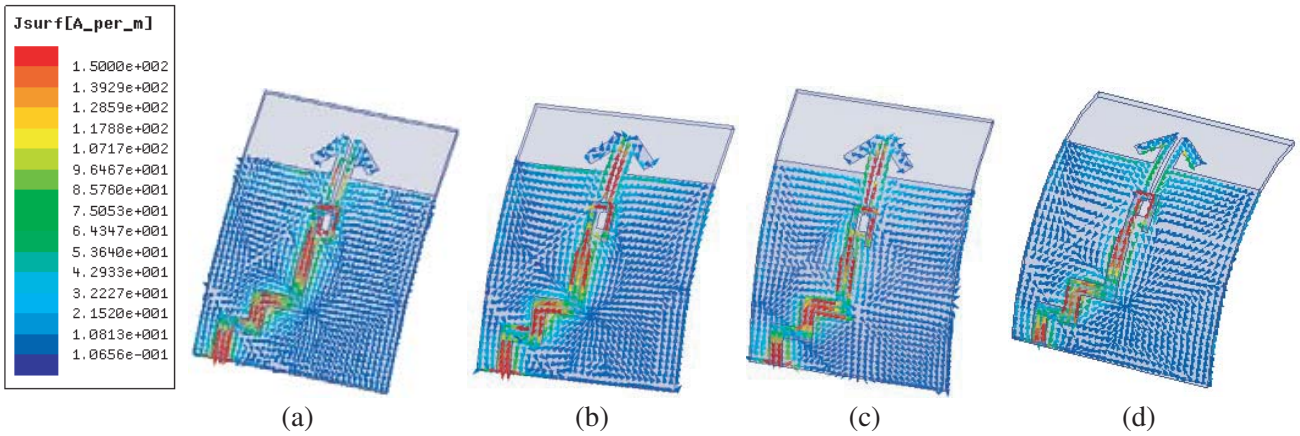


**Figure 17.** Current distribution of conformal models at 33 GHz. (a) 30°. (b) 45°. (c) 60°. (d) 90°.

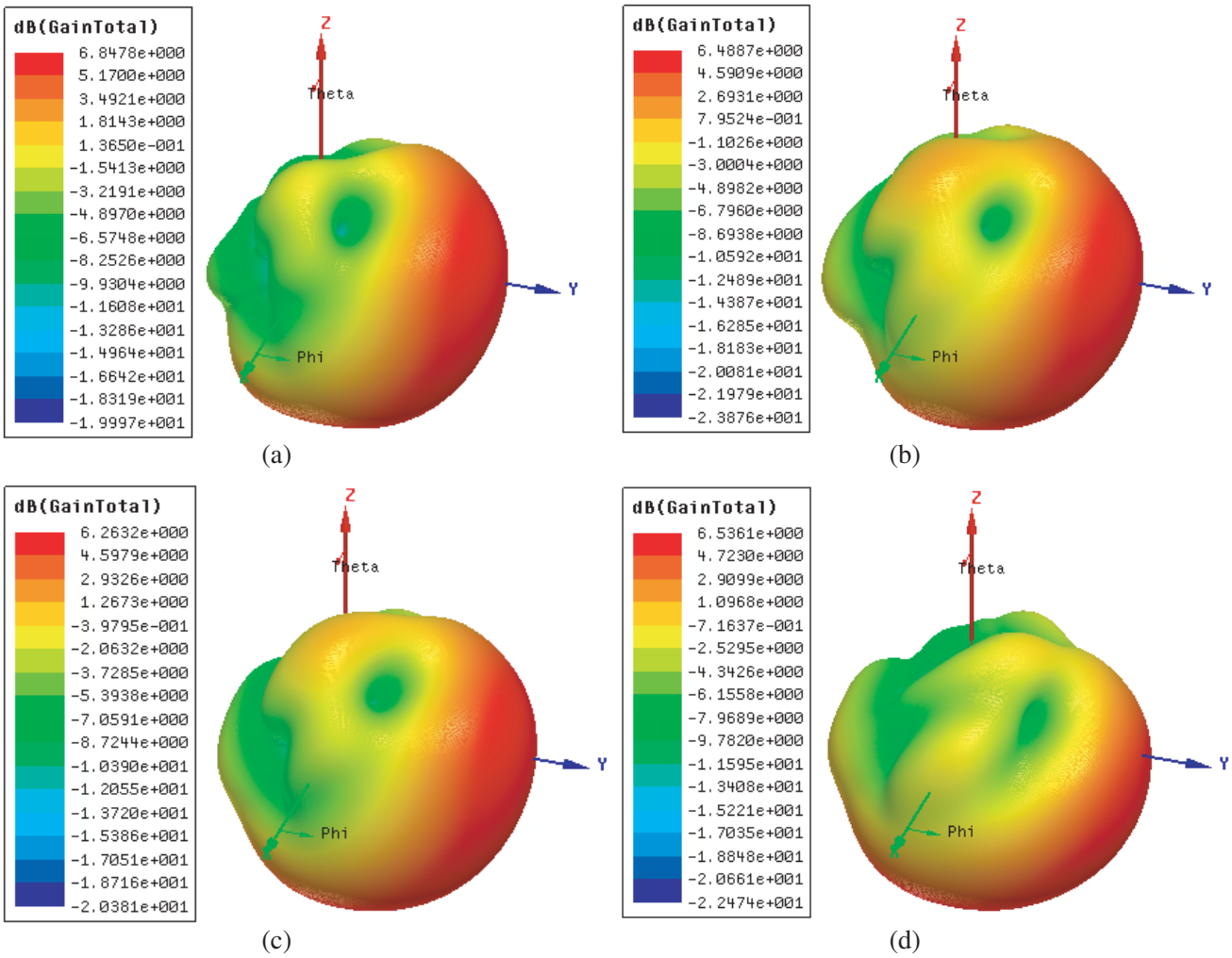


**Figure 18.** 3D Gain plots of conformal models at 33 GHz. (a) Conformal at 30°. (b) Conformal at 45°. (c) Conformal at 60°. (d) Conformal at 90°.

The measured reflection coefficient characteristics for conformal models at 60° and 90° are represented in Fig. 16. The conformal model at 60° operates for frequency range of 29.21 to 42.63 GHz and 50.9 to 52.2 GHz with bandwidths of 13.42 GHz and 1.3 GHz. The conformal model at 90° operates from 25 to 35.65 GHz, 38.92 to 40.7 GHz and 51.2 to 53.1 GHz. There is a shift in the frequency band for conformal model at 60° by which 28 GHz is not achieved, and a notch is observed from 35.65 to 38.92 GHz for conformal model at 90°, and hence 37 GHz is not achieved.

The current distribution for the four conformal models is observed at 33 GHz in HFSS as shown in Fig. 17. From these distributions it can be observed that angled dipole acts as the radiating element and not the microstrip feedline with balun. It appears identical for all the conformal models with small deviations. The maximum current distribution is observed along the staircase balun structure and comparatively less for model at 90°. For conformal models at 45° and 60°, more current is observed at dipoles than models at 30° and 90°.

Figure 18 represents the simulated 3D gain plots of conformal models at 33 GHz. The conformal models projecting a little bit high gain in dB over the planar (unbent) antenna model. A gain of 6.84 dB is achieved for conformal at 30°. The gain for conformal model at 45° is 6.48 dB; at 60° it is 6.26 dB; at 90° it is 6.53 dB. It can be concluded from the obtained results that the conformal models are in good agreement in gain.

The measured $E$-plane and $H$-plane patterns of conformal models at 33 GHz are illustrated in Figs. 19(i) and (ii), respectively. The obtained $E$-plane and $H$-plane patterns are almost identical for 30°, 45° and 60° conformal models. The $H$-plane patterns exhibit omnidirectional pattern, and the $E$-plane patterns are directive in nature.

Comparison of antenna parameters with and without bending: The developed conformal models are compared with the un-bended one in Table 3. The parameters considered for comparison are operating bands (GHz), bandwidth (GHz), useful 5G bands (GHz) and gain (dB) at 33 GHz.

**Table 3.** Comparison of conformal models.

| Antenna Model | Operating Bands (GHz) | Bandwidth (GHz) | Achieved 5G Bands (GHz) | Gain (dB at 33 GHz) |
|---|---|---|---|---|
| Without bending | 24.3–41.95, 49.91–52.15 | 17.65, 2.24 | 28, 33, 37, 39, 51 | 4.24 |
| Conformal at 30° | 25.62–42.51, 49.53–52.05 | 16.33, 2.52 | 28, 33, 37, 39, 51 | 6.84 |
| Conformal at 45° | 25.59–42.51, 50.55–53 | 16.92, 2.45 | 28, 33, 37, 39, 51 | 6.48 |
| Conformal at 60° | 29.21–42.63, 50.9–52.2 | 13.42, 1.3 | 33, 37, 39, 51 | 6.26 |
| Conformal at 90° | 25–35.65, 38.92–40.7, 51.2–53.1 | 10.65, 1.78, 1.9 | 28, 33, 39 | 6.53 |

From Table 3, it can be concluded that conformal models have better gain over the model without bending. Though there is a minor shift in the frequency bands for conformal models at 30° and 45°, the required frequencies for vehicular communications, i.e., 28 GHz, 33 GHz, 37 GHz, 39 GHz are still achieved. As the conformal models at 60° and 90° do not satisfy the entire frequency bands required for vehicular communications, only the models at 30° and 45° are preferable. Thus, the proposed antenna is well suited for vehicular communications as it can be embedded on vehicles at different structures supporting 30° and 45° bends.

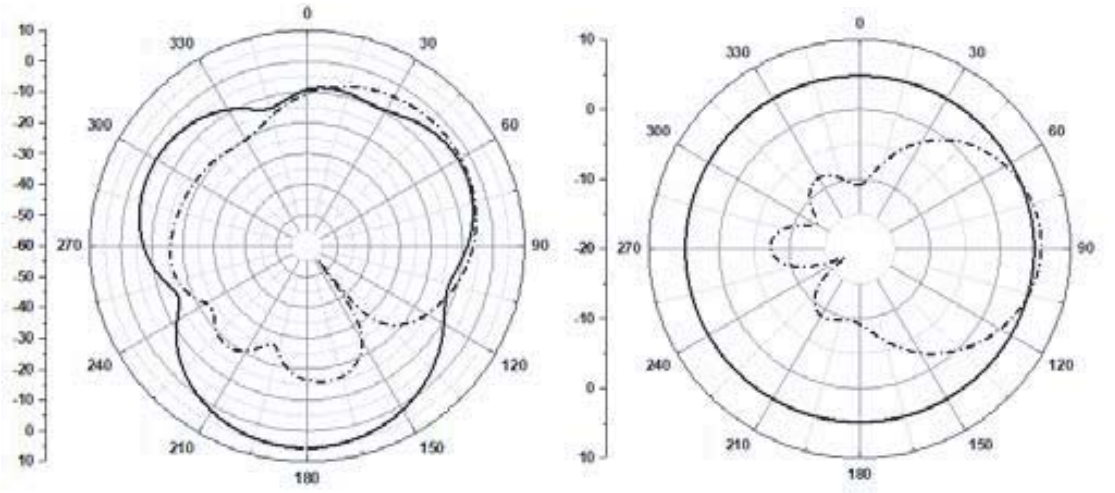


(i) (a) (ii)

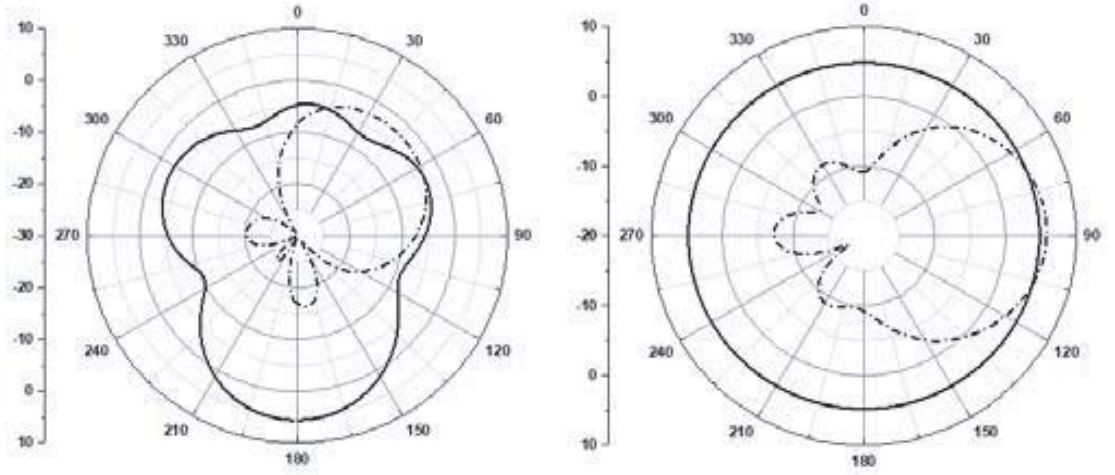


(i) (b) (ii)

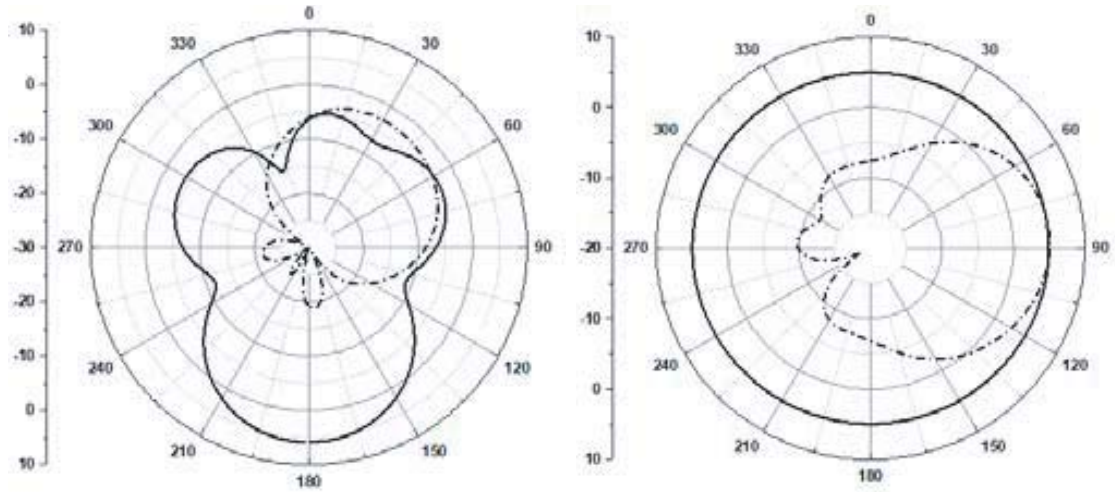


(i) (c) (ii)

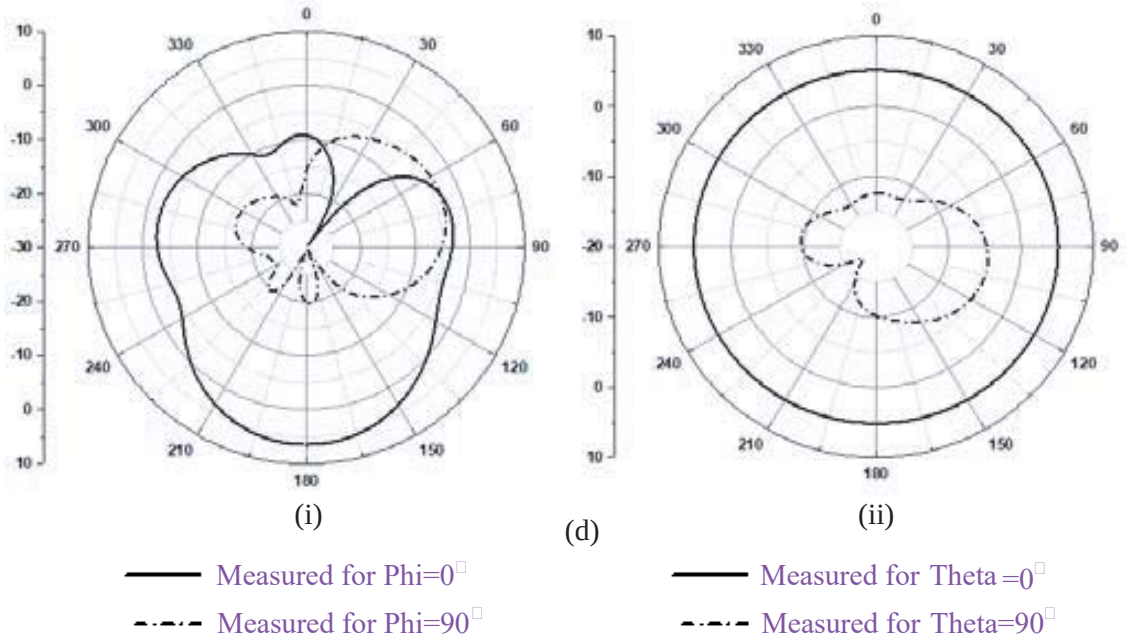


**Figure 19.** Measured radiation patterns in (i) *E*-Plane and (ii) *H*-Plane for conformal models at 33 GHz. (a) Conformal at 30°. (b) Conformal at 45°. (c) Conformal at 60°. (d) Conformal at 90°.

## 6. VEHICULAR PLACEMENT

The designed antenna model is placed on the top side of the front wind glass of the vehicle and simulated using ANSYS SAVANT tool. The obtained results at an angle of 30° on the vehicle body are presented in Fig. 20. The three-dimensional radiation view for normalized power density in Fig. 20(a) and the gain in Fig. 20(b) can be witnessed here. In the case of normalized power density, the total instantaneous radiated power leaving the surface of the vehicle structure is found by integrating the instantaneous Poynting vector over the surface. It can be viewed that most of the power is radiated in the forward

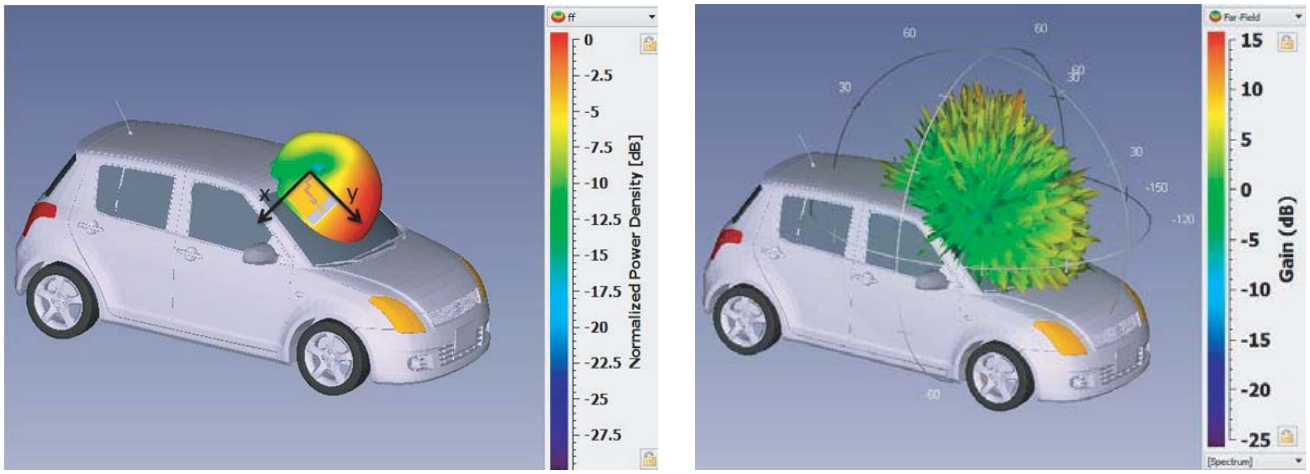


**Figure 20.** Simulation results in SAVANT at 33 GHz. (a) Normalized power density in dB. (b) 3D gain plot in dB.

direction (along the $y$-axis of the antenna) of the vehicle and very little in the backward direction and into the vehicle. When antenna gain plot is observed, a value of 5.9 dB is attained in the vehicular body placement condition. This slight variation of gain is due to the interference of the antenna radiation with the metallic structure of the vehicle body.

## 7. CONCLUSION

A novel printed dipole antenna with a staircase structured offset fed and dipole like defected ground structure is presented in this paper. The designed antenna attains a broad operating band from 24.3 to 41.95 GHz that covers the 5G bands 28 GHz, 33 GHz, 37 GHz and 39 GHz suitable for vehicular communications in connected vehicles through IoT. It is also working at 51 GHz band, which is suitable for future satellite applications. The proposed antenna has a compact size of $10 \times 13 \times 0.254\,\text{mm}^3$ on a liquid crystal polymer substrate and possesses several superior parameters, impedance bandwidth, peak gain and radiation efficiency. The developed conformal models are best suitable for vehicular body placement and subsequent communications, 5G based wireless communications and IoT applications.

## ACKNOWLEDGMENT

Authors would like to thank the Department of ECE of KLEF and VFSTR for their encouragement during this work and DST for technical support through ECR/2016/000569, and EEQ/2016/000604.

## REFERENCES

1. Agiwal, M., A. Roy, and N. Saxena, "Next generation 5G wireless networks: A comprehensive survey," *IEEE Communications Surveys & Tutorials*, Vol. 18, No. 3, 1617–1655, Third Quarter 2016.
2. Wang, T., G. Li, B. Huang, Q. Miao, J. Fang, P. Li, H. Tan, W. Li, J. Ding, J. Li, and Y. Wang, "Spectrum analysis and regulations for 5G," *5G Mobile Communications*, W. Xiang et al. (eds.), 27–50, Springer International Publishing Switzerland, 2017.
3. Choi, J., V. Va, N. González-Prelcic, R. Daniels, C. R. Bhat, and R. W. Heath, Jr., "Millimeter wave vehicular communication to support massive automotive sensing," *IEEE Communications Magazine*, Vol. 54, No. 12, 160–167, December 2016.
4. Dong, P., T. Zheng, S. Yu, H. Zhang, and X. Yan, "Enhancing vehicular communication using 5G-enabled smart collaborative networking," *IEEE Wireless Communications*, Vol. 24, No. 6, 72–79, December 2017.
5. Ojaroudiparchin, N., M. Shen, and G. F. Pedersen, "Investigation on the performance of low-profile insensitive antenna with improved radiation characteristics for the future 5G applications," *Microwave and Optical Technology Lett.*, Vol. 58, No. 9, 2148–2151, September 2016.
6. Nor, N. M., M. H. Jamaluddin, M. R. Kamarudin, and M. Khalily, "Rectangular dielectric resonator antenna array for 28 GHz applications," *Progress In Electromagnetics Research C*, Vol. 63, 53–61, 2016.
7. Lin, W., R. W. Ziolkowski, and T. C. Baum, "28 GHz compact omnidirectional circularly polarized antenna for device-to-device communications in the future 5G systems," *IEEE Transactions on Antennas and Propagation*, Vol. 65, No. 12, 6904–6914, December 2017.
8. Alhalabi, R. and G. Rebeiz, "High-efficiency angled-dipole antennas for millimeter-wave phased array applications," *IEEE Transactions on Antennas and Propagation*, Vol. 56, No. 10, 3136–3142, October 2008.
9. Ta, S. X. and I. Park, "Broadband printed-dipole antennas for millimeter wave applications," *Proc. Int. Symp. IEEE Radio Wireless*, 65–67, Phoenix, AZ, USA, January 2017.
10. Ta, S. X., H. Choo, and I. Park, "Broadband printed-dipole antenna and its arrays for 5G applications," *IEEE Antennas Wireless Propag. Lett.*, Vol. 16, 2183–2186, May 2017.

11. Jilani, S. F. and A. Alomainy, "A multiband millimeter-wave two-dimensional array based on enhanced Franklin antenna for 5G wireless systems," *IEEE Antennas Wireless Propag. Lett.*, Vol. 16, 2983–2986, September 2017.
12. Yang, B., "A compact integrated bluetooth UWB dual-band notch antenna for automotive communication," *International Journal of Electronics and Communications*, Vol. 80, 104–113, 2017.
13. Madhav, B. T. P., T. Anilkumar, and K. Sarat, "Transparent and conformal wheel-shaped fractal antenna for vehicular communication applications," *International Journal of Electronics and Communications*, Vol. 91, 1–10, 2018.
14. Ramya, R. and T. Rama Rao, "Design and performance analysis of a penta-band spiral antenna for vehicular communications," *Wireless Pers. Commun.*, Springer, March 2017.
15. Mondal, T., S. Samanta, R. Ghatak, and S. R. Bhadra Chaudhuri, "A novel tri-band hexagonal microstrip patch antenna using modified Sierpinski fractal for vehicular communication," *Progress In Electromagnetics Research C*, Vol. 57, 25–34, 2015.
16. Wong, H., K. K. So, and X. Gao, "Bandwidth enhancement of a monopolar patch antenna with V-shaped slot for car-to-car and WLAN communications," *IEEE Transactions on Vehicular Technology*, Vol. 65, No. 3, 1130–1136, March 2016.
17. Balanis, C. A., *Antenna Theory: Analysis and Design*, 3rd Edition, New Jersey, Wiley, 2005.
18. Kraus, J. D., R. J. Marhefka, and A. S. Khan, *Antennas and Wave Propagation*, 4th Edition, Mc-Graw Hill, 2015.